Review

Jeffrey E. Melzer* and Euan McLeod*

3D Nanophotonic device fabrication using discrete components

Abstract: Three-dimensional structure fabrication using discrete building blocks provides a versatile pathway for the creation of complex nanophotonic devices. The processing of individual components can generally support high-resolution, multiple-material, and variegated structures that are not achievable in a single step using top-down or hybrid methods. In addition, these methods are additive in nature, using minimal reagent quantities and producing little to no material waste. In this article, we review the most promising technologies that build structures using the placement of discrete components, focusing on laser-induced transfer, light-directed assembly, and inkjet printing. We discuss the underlying principles and most recent advances for each technique, as well as existing and future applications. These methods serve as adaptable platforms for the next generation of functional three-dimensional nanophotonic structures.

Keywords: 3D fabrication; building blocks; nanoassembly; nanofabrication; nanophotonics.

1 Introduction

The ability to rapidly fabricate complex three-dimensional (3D) structures with nanoscale resolution is an enabling technology for many applications throughout the physical and life sciences. In photonics, metamaterials rely on the patterning of multiple materials at subwavelength scales to achieve exotic optical properties like negative refractive index, optical magnetism, or near-zero dielectric permittivity [1]. These materials can be used to create more versatile polarization controllers, superresolution imagers or other devices based on transformation optics [2–4]. Photonic integrated circuits are primarily composed of planar waveguides and functional structures, however 3D integration is often necessary to package and couple light in and out of these devices or to improve the density of functional components [5, 6]. Many photonic biosensors also rely on 3D nanostructuring. Surface-enhanced Raman scattering (SERS) can be used to acquire spectroscopic information of individual molecules in the presence of roughened or nanostructured metallic surfaces [7]. Whispering gallery mode biosensors can also benefit from the integration of nanophotonic elements to facilitate greater interaction between the analyte and the evanescent whispering gallery mode field, as well as for coupling light in and out [8–10]. High pixel density image sensors also depend on the 3D integration of the electronic elements for pixel readout as well as optical structures to guide light to the pixel active area. For multifunctional image sensors that capture more information than just red, green, and blue values, 3D superstructures on the pixel surface can provide additional functionality like angle sensitivity, polarimetric sensing, or high-performance spectral filters [11–13]. In addition to optoelectronics, pure electronic applications can also benefit from 3D nanofabrication to realize 3D integrated circuit architectures which overcome the computational bottleneck associated with data-intensive operations [14]. Throughout the following discussion, we investigate 3D nanofabrication techniques in the context of nanophotonics, but note that the methods we discuss are not restricted to any specific application.

The design and theory of novel and complex nanophotonic devices has rapidly grown over the past few decades, creating a gap between what can be proposed and simulated versus what is experimentally feasible. In practice, it can be challenging to fabricate devices with the required level of accuracy and precision. To address these challenges, several methods for 3D nanofabrication have been established or significantly improved over the last few years, including techniques such as direct laser writing [15–22], and self-assembly [23–26], among others. Direct laser writing, most often in the form of two-photon

*Corresponding authors: Euan McLeod and Jeffrey E. Melzer, Wyant College of Optical Sciences, University of Arizona, Tucson, AZ, USA, E-mail: euanmc@optics.arizona.edu (Euan McLeod), jmelzer@optics.arizona.edu (Jeffrey E. Melzer). https://orcid.org/0000-0002-6327-364 (E. McLeod). https://orcid.org/0000-0002-7564-4455 (J.E. Melzer)

polymerization (TPP), is currently one of the most widely-used 3D nanofabrication methods. In this technique, a laser beam is tightly focused within a photoresin and scanned in three dimensions to polymerize a volume of material, corresponding to the desired 3D nanostructure. Due to the nonlinear absorption mechanism responsible for polymerizing the resin, 3D confinement and high spatial resolution beyond the diffraction limit is achievable, typically on the order of 100 nm in both the lateral and axial dimensions [15, 20]. Furthermore, fast scan speeds up to 100 mm/s enable efficient processing of extended structures. However, TPP, along with many other existing fabrication technologies, lacks flexibility in incorporating multiple materials using a single process, which is a highly desirable characteristic for an ideal 3D nanofabrication technique.

In this review, we focus exclusively on three alternative methods that utilize discrete, potentially nanoscale, components as building blocks with few material restrictions, permitting the fabrication of high-resolution 3D structures with complex geometry and variegated materials. Specifically, we consider laser induced transfer (LIT), light directed assembly, and inkjet printing. We believe that these three approaches can extend the range of experimentally-feasible 3D nanostructures. The main advantage of fabrication methods based on discrete components is the freedom with which variegated materials can be incorporated, especially nanoscale materials that have been preprocessed before their incorporation into a

larger structure. For example, quantum dots or biochemically functionalized particles are discrete components that are straightforward to synthesize in large quantities and can be positioned using the techniques we discuss here. However, they would be difficult to fabricate in specific locations on a 3D structure using monolithic techniques like direct laser writing or lithography, which work from a bulk material preform and only structure a single material at a time. While self-assembly techniques also utilize discrete components, they do not permit the precise positioning in arbitrary complex geometries.

Figure 1 illustrates the writing speeds and minimum feature sizes that have been achieved with these techniques. In general, desirable approaches maximize writing speed while minimizing lateral feature size; however, these two parameters are often positively correlated due to fundamental physical limitations. For comparison, Figure 1 also includes a data point for two-photon polymerization, which is quite fast and high resolution compared to the other techniques, indicating a direction for future improvement for the methods based on discrete components.

In the following sections, we outline each of these methods, demonstrating their 3D multimaterial nanofabrication capabilities, and discuss existing nanophotonic devices that have already been fabricated using these approaches. Following our exploration of each technique, we compare the practical advantages and disadvantages of each method, providing additional insight on the most suitable applications for each technique.
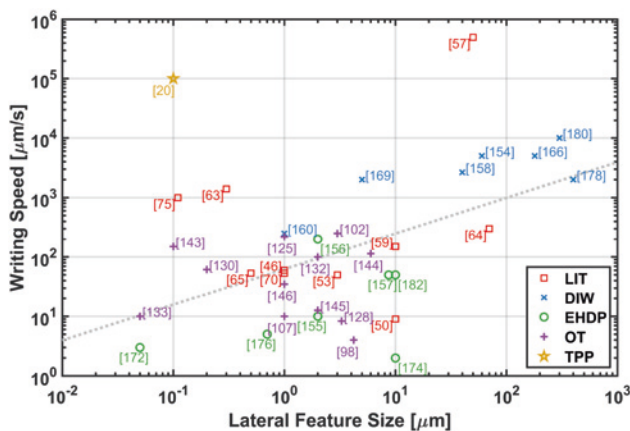

Figure 1: Feature size vs. writing speed for laser induced transfer (LIT), direct ink writing (DIW), electrohydrodynamic printing (EHDP), optical tweezers (OT), and two photon polymerization (TPP). Optical tweezers belong to the class of light directed assembly techniques, while direct ink writing and electrohydrodynamic printing are subcategories of inkjet printing. The dotted line is the best fit line of all the data points (excluding TPP), illustrating the positive correlation between feature size and writing speed.

2 Laser induced transfer

The LIT process uses a pulsed laser to transfer material from a donor substrate to a receiving substrate. While the underlying mechanism of LIT varies depending on the physical state of the donor material (e.g., solid, liquid, or paste), the general principle relies on laser absorption in the donor medium [27–29]. In the case of a liquid phase donor layer (Figure 2A), laser absorption in the liquid film causes a cavitation bubble to form, ultimately leading to the ejection of a droplet or liquid jet of material traveling toward the substrate [18, 30–33]. In the case of a solid absorbing donor layer, laser absorption at the interface between the donor layer and donor substrate causes a rapid increase in temperature and pressure, thereby breaking off the irradiated voxel and pushing it towards the substrate [27]. In each of these scenarios, we assume that the donor material is absorptive at the wavelength used by the pulsed laser; however, it is also possible to transfer
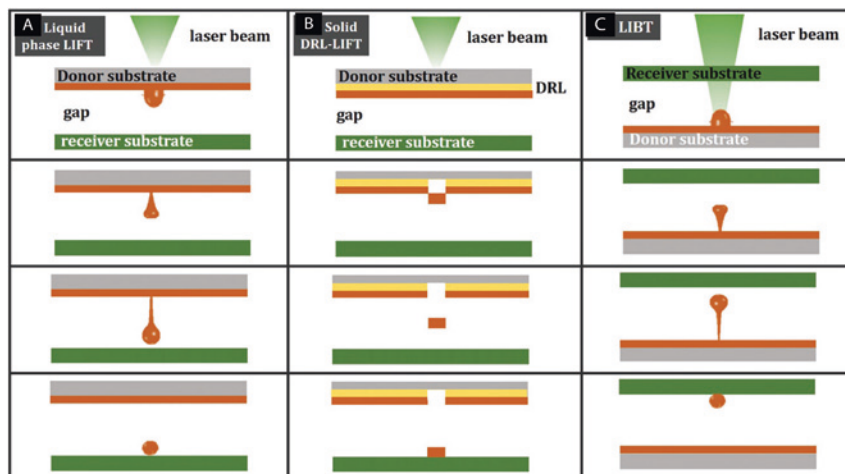
Figure 2: Illustrations of typical LIT configurations: (A) laser induced forward transfer (LIFT) with a liquid phase donor layer, (B) LIFT with a solid donor layer and dynamic release layer (DRL), and (C) laser induced backward transfer (LIBT). Reprinted with permission from Ref. [31].

materials which are either transparent or sensitive to laser radiation by incorporating a sacrificial absorbing layer between the donor material and donor substrate, typically referred to as a dynamic release layer, or DRL (Figure 2B) [27, 28, 31, 34, 35]. If the DRL is a solid polymer, then it may undergo rapid elastic and plastic deformation without being completely vaporized or ablated by the laser pulse, facilitating transfer of the donor material without the unwanted transfer of the DRL material [36–38].

There are many advantages and disadvantages associated with the liquid and solid phase donor alternatives. For example, solid phase layers are far more stable than liquid phase layers; the solvent incorporated in liquid phase layers will naturally evaporate over time, significantly affecting the optimal LIT process parameters, as well as the transferred material characteristics [18, 27, 39, 40]. However, the use of solid donor layers can generate debris and also induce the formation of a shock wave, which can disrupt the receiver substrate and/or the transferred voxel [35, 41]. One approach to extract the respective advantages of liquid phase and solid phase donor media is to perform liquid-phase printing using a solid donor layer. This can be achieved by using a thin solid donor film and sufficient laser fluence in order to first melt and then transfer the voxel to the substrate [42]. Alternatively, this can be achieved using a dual-laser setup, in which one laser first melts the solid film and the other laser then initiates the jetting process [43].

In addition to variation in donor material phase, LIT can be categorized according to the direction of material transfer. In laser induced forward transfer (LIFT, Figure 2A/B) the transferred material travels in the same direction as the laser pulse, whereas in laser induced backward transfer (LIBT, Figure 2C), the material is transferred in the opposite direction. In LIBT, the laser passes through the receiving

substrate to focus onto the donor substrate [33, 44]. LIFT provides an advantage over LIBT due to greater versatility in the choice of the receiving substrate, as substrate transparency is not critical [45].

A major attraction of the LIT technique is its broad material compatibility. It has been demonstrated with a variety of donor materials, including metals [32, 33, 44–50], polymers [51, 52], chalcogenides [53, 54], metal oxides [55, 56], and biological media [57–59]. In addition to the diversity of donor material, the LIT approach facilitates control over the size and shape of the transferred material, or voxel, through tuning the fluence, pulse duration, wavelength, and width of the incident laser beam [17, 27, 28, 34]. By mounting the donor substrate and/or receiving substrate on a 3-axis stage, it is possible to fabricate 2D and 3D structures using the LIT process.

Significant work has been performed to enable LIT to be used to fabricate 2D and 3D nanostructures (Figure 3). Zywietz et al. used LIBT to print highly uniform silicon nanoparticles using a silicon-on-insulator wafer with 50 nm thick solid silicon layer as the donor substrate. The silicon was transferred using a laser with 50 fs pulse length and 800 nm center wavelength. The pulse energy was adjusted to tailor the diameter of the fabricated silicon nanoparticle between 165 and 240 nm [60, 62]. The high uniformity and degree of control was attributed to the backward nature of the transfer process. Visser et al. demonstrated the fabrication of high aspect ratio pillars of copper using LIFT. The 80 μm tall pillar shown in Figure 3C was fabricated using a 515 nm laser with 6.7 ps pulse duration to eject droplets from a 200 nm copper film, which yielded micron-sized droplets due to the picosecond length pulse duration [49]. Sametoglu et al. printed chromium nanoparticles as small as 70 nm in diameter using LIFT with a thin 20 nm donor layer (Figure 3D–F). This was achieved using 130 fs laser pulses
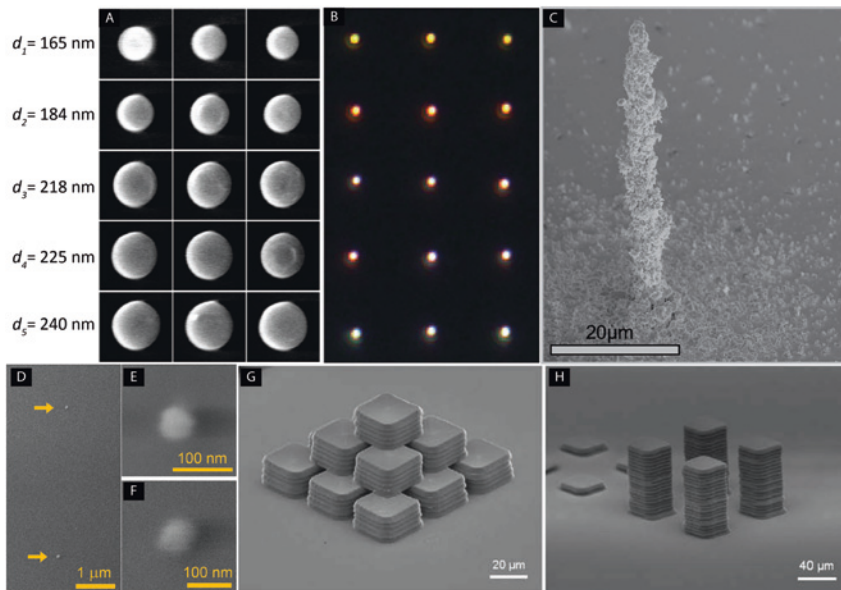
Figure 3: 2D and 3D nanofabrication using LIT. (A–B) SEM images (A) and darkfield microscopy (B) of silicon nanoparticles fabricated with LIBT using different laser pulse energies. Different colors are seen in the dark field image due to the Mie resonances of the nanoparticles. Reprinted with permission from Ref. [60]. (C) Copper pillar with a high aspect ratio of ~15 fabricated using LIFT. Reprinted with permission from Ref. [49]. (D–F) SEM of transferred chromium nanoparticles with diameter ~70 nm. Reprinted with permission from Ref. [61]. (G–H) LIFT of high aspect ratio micro pyramid and micro pillars printed using silver nanopaste. Reprinted with permission from Ref. [40].

at a wavelength of 800 nm [61]. In a final example, Wang et al. printed high aspect ratio microstructures consisting of many rectangular voxels of silver nanoparticle paste using a 355 nm laser with 30 ns pulse duration (Figure 3G/H) [40]. This demonstrates the versatility of voxel shape, range of feature sizes, and the 3D fabrication capability of the LIT process.

Figure 4: Dependence of lateral feature size in LIT as a function of (A) donor film thickness, (B) pulse duration, and (C) laser fluence.

The main parameters that influence the LIT process are the laser fluence, laser pulse duration, donor film thickness, donor viscosity, and donor-receiver spacing. The dependencies of voxel feature size on laser fluence, pulse duration, and donor film thickness are shown in Figure 4 based on the collated results from a large number of different studies [32, 39, 45, 46, 50, 53, 57, 58, 60, 61, 63–71]. Note that we only consider studies that report all four of these values, and therefore these results do not encompass the full parameter space existing in the literature. In general, we find that independent of donor material phase, a strong positive correlation exists between the donor film thickness and the resulting voxel lateral feature size, indicating that it is a critical parameter in minimizing printing resolution. In addition, we note that longer laser pulse durations generally correspond to larger voxel sizes. The effect of laser fluence on voxel size is less clear due to differing confounding factors in the various studies, such as differing material absorption, wavelength, pulse duration, and donor thickness.

Beyond the ability to fabricate nanoscale voxels, it is also important to consider process efficiency, which is influenced primarily by writing speed and positioning accuracy. While writing speeds in the literature vary greatly from the order of 10s of μm/s to 100s of mm/s, we find that this parameter is generally limited by the technical limits of the specific system hardware (e.g. stage translation speeds, laser repetition rate, etc.) rather than any fundamental physical restriction. One specific exception to this general trend arises in the case of a liquid donor film, in which adjacent liquid jets may interact if
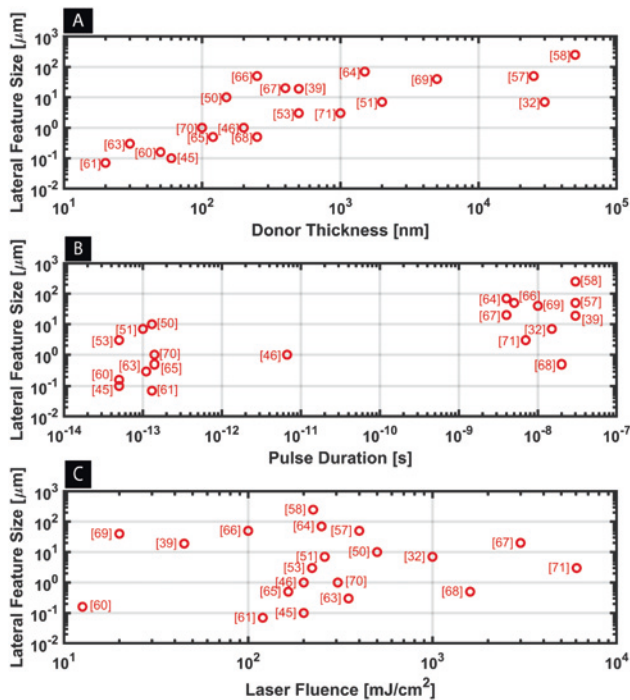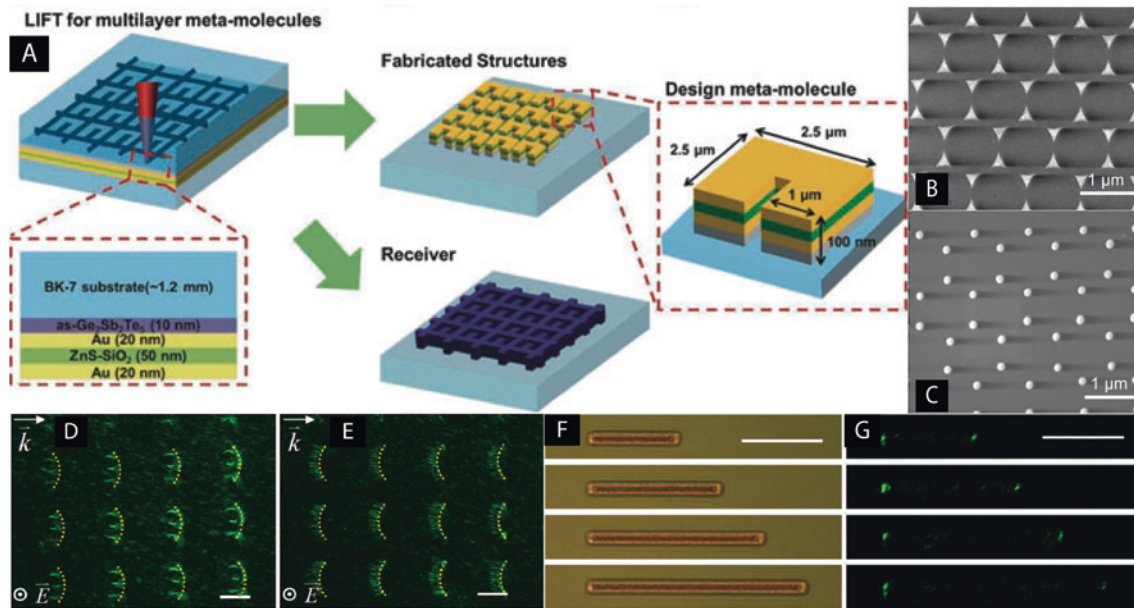
Figure 5: LIT in plasmonics and metamaterial fabrication. (A) Schematic illustrating the LIFT process for fabrication of a split ring resonator array. Reprinted with permission from Ref. [70]. (B-C) LIBT of a spherical gold nanoparticle array with SEM images of the donor substrate before transfer (B) and the receiving substrate after transfer (C). The pattern on the donor substrate is achieved using nanosphere lithography with physical vapor deposition of a gold film. Reprinted with permission from Ref. [75]. (D–E) Dark field images of surface plasmon polaritons scattering by concave (D) and convex (E) nanofences composed of gold nanoparticles. The green lines seen in the images correspond to a 532 nm laser interacting in-plane with these nanostructures. Scale bars are 10 μm. Reprinted with permission from Ref. [76]. (F–G) Optical microscope images of gold plasmonic waveguides with varying length (F) and dark-field microscopy demonstrating the guiding properties of the waveguides (G). Scale bars are 10 μm. Reprinted with permission from Ref. [76].

time delays between transfer events are below ~100 μs [34, 72]. Approaches which may be used to improve the process efficiency of LIT techniques include beam shaping with a digital micromirror device (DMD) or microlens array, which parallelizes the fabrication process [73, 74]. The quantitative positioning accuracy of the LIT process is widely unreported in the literature, and hence we cannot comment explicitly on the range of accuracy expected in these techniques.

In the following sections, we discuss applications of LIT that have already been realized for the fabrication of plasmonic structures, metamaterials, and light emitting diodes (LEDs).

2.1 Plasmonics and metamaterials

Several studies have focused on using LIT as a fabrication technique for plasmonic and metamaterial structures (Figure 5) [44, 45, 50, 65, 70, 75–77]. Tseng et al. used LIFT to print split-ring resonators from a solid phase multilayer donor film with a laser wavelength of 800 nm and pulse duration of 140 fs [70]. This study highlights another advantage of the LIT technique, namely that

multiple layers can be transferred simultaneously. The work performed here is also unique in that the desired product is fabricated in the donor layer rather than on the receiving substrate (Figure 5A). The resulting metamaterial pattern on the donor substrate is generated by transferring the inverse pattern onto the receiver substrate, similar to the concept of a negative resist in a photolithography process.

Aristov et al. used LIBT to form a plasmonic array of spherical gold nanoparticles [75]. They first used nanosphere lithography to fabricate a hexagonal array of triangular structures by depositing a 45 nm gold film using physical vapor deposition. The triangular pixels were subsequently transferred to a polydimethylsiloxane (PDMS) receiver substrate using a femtosecond laser, ultimately resulting in spherical droplets due to the effects of surface tension after melting by the laser. In addition to split ring resonators, Tseng et al. also fabricated gold plasmonic nanofences and plasmonic waveguides using LIFT [76]. The fabricated nanofences effectively focused and defocused surface plasmon polaritons, as demonstrated in Figure 5D/E. Further, the gold plasmonic waveguides successfully propagated 532 nm laser radiation, as depicted in Figure 5G.
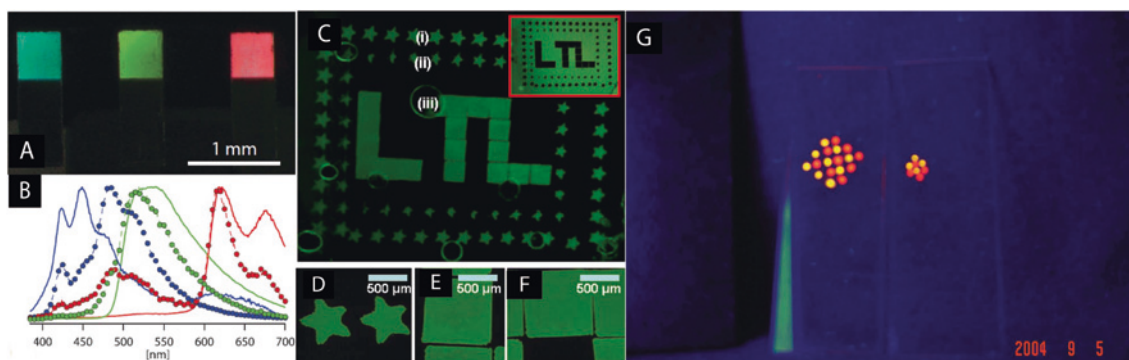
Figure 6: LIT of light emitting diode material. (A–B) Tri-color pixels imaged in a light microscope (A) and corresponding electroluminescence spectra (B) of the laser-printed pixels (dashed lines with circular markers) and conventionally fabricated devices (solid lines). Reprinted with permission from Ref. [80]. (C–F) Fluorescent images of Alq$_3$ transferred using LIFT with masks to vary the pattern shape. Reprinted with permission from Ref. [66]. (G) Image of 6 × 6 matrix of alternating nanocrystal quantum dots under UV illumination. Reprinted with permission from Ref. [81].

2.2 Light emitting diodes

Several groups have investigated LIT as an approach to fabricate LEDs (Figure 6) [66, 77–81]. Although these results do not explicitly demonstrate nanoscale fabrication, we believe the material diversity and control over voxel shape make these worthwhile inclusions in this article. Furthermore, the results shown here for LED fabrication can certainly be extended to smaller length scale devices. Stewart et al. printed red, green, and blue polymer LED pixels using three different multilayered donor substrates, fabricating OLED pixels with visible spectra comparable to conventionally-fabricated OLEDs. The multilayer donor substrate contained a DRL, along with a layer of light emitting polymer and an aluminum cathode [80]. Ko et al. similarly used a DRL, consisting of silver nanoparticles, in order to transfer the OLED material tris-(8-hydroxyquinoline)Al (Alq$_3$) to a receiving substrate [66]. Xu et al. used

LIFT to print pixels with an active layer composed of different nanocrystal quantum dots (NQD), demonstrating the feasibility of fabricating NQD arrays [81].

3 Light directed assembly

Light directed, or driven, assembly (LDA) encompasses several techniques that rely on an optical beam to generate a force, which enables the positioning of various objects. The generated force can be the optical force from the beam itself or an induced force at an interface. The main variants of LDA include techniques such as opto-electronic tweezers (OET) [82–85], opto-thermophoretic tweezers (OTT) [86–92], bubble pen lithography (BPL) [93–96], and optical tweezers (OT) [97–111]. The first three listed techniques—OET, OTT, and BPL—rely on the presence of a substrate to generate the required force.
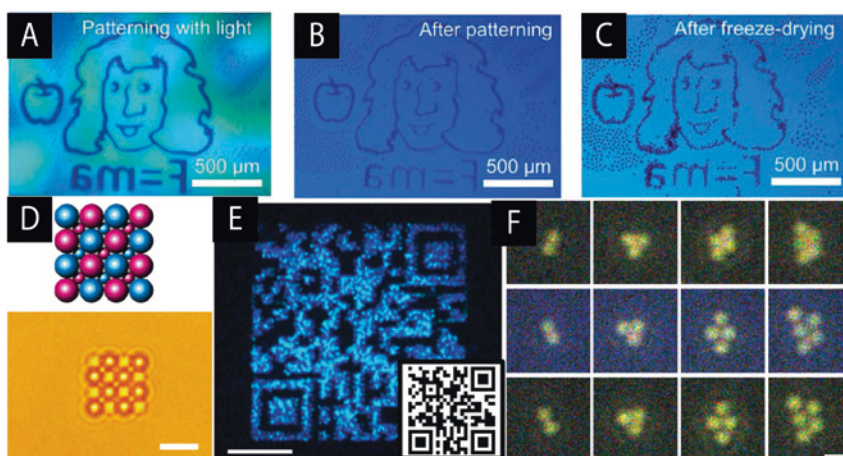

Figure 7: Examples of 2D LDA fabrication methods. (A-C) Image of Isaac Newton assembled with 10 μm PS beads using OET. Reprinted with permission from Ref. [82]. (D) Superlattice consisting of 2 μm PS, 0.96 μm PS, 2 μm silica, and 1 μm silica beads, assembled using OTT. Scale bar is 5 μm, blue spheres indicate silica, and magenta spheres indicate PS. Reprinted with permission from Ref. [89]. (E) 80 × 80 μm QR code printed with blue quantum dots via BPL. Scale bar is 25 μm. Reprinted with permission from Ref. [94]. (F) 150 nm gold nanospheres assembled using optical binding forces and immobilized with photopolymerization. Scale bar is 1 μm. Reprinted with permission from Ref. [112].

In OET (Figure 7A–C), a sample cell containing the desired building blocks is sandwiched between two electrodes with an applied AC electrical bias. The bottom electrode is coated with a photoconductive layer, such that the illumination of patterned light fields on the bottom electrode surface generates a predictable electric field within the sample cell. This electric field will interact with and induce dipole moments in the nearby objects, exerting a dielectrophoretic force on the objects [85]. In the case of OTT (Figure 7D), the main requirement for the sample chamber is an optothermally responsive bottom substrate, such as a thin layer of metal. A laser illuminates the metal film, leading to localized heating, which establishes a thermal gradient in the sample cell exerting a thermophoretic force on objects in the cell [88–90]. In BPL (Figure 7E), a laser beam is focused on to a plasmonic substrate with sufficient energy to form a microbubble on the surface. The presence of the bubble leads to convective forces which tend to direct objects toward the bubble-substrate junction [93, 95].

Various additional LDA methods exist which use a combination of these effects, among others, to assemble objects [108, 112–119]. Figure 7F, for example, depicts different arrangements of 150 nm gold spheres that were assembled using optical binding forces [112]. A circularly polarized laser operating at 800 nm was used to form the plasmonic structures, followed by a UV laser to immobilize the pattern via photopolymerization of a water-soluble photopolymer. The optical binding force should promote uniform inter-particle spacing on the order of the laser wavelength, thereby providing a method for the directed assembly of large plasmonic arrays.

Another technique, demonstrated by Li et al. uses the scattering forces of a laser in conjunction with the photothermal properties of a thin surfactant layer in order to position nanoparticles on a 2D substrate [119]. In this novel technique, termed optothermally-gated photon nudging (OPN), the laser beam simultaneously directs the particles and induces a localized phase transition in the solid surfactant layer, which permits motion of the particle. In the absence of the laser, the surfactant layer remains solid, fixing the particles in place.

While each of the techniques described thus far has the advantage of being able to manipulate a broad range of materials and object sizes and shapes using a low-power optical beam, a frequent disadvantage is the necessity of a specific substrate to generate the required force. As such, these techniques are predominantly restricted to the patterning of objects in the 2D plane, severely limiting their utility for 3D nanofabrication.

For the remainder of this section on light directed assembly, we focus exclusively on OT, an approach which enables full 3D positioning capability, yet still boasts many of the advantages of the aforementioned 2D LDA techniques, albeit often requiring higher laser powers. In a typical OT setup, a laser beam is focused to a tight spot using a high-power objective lens. When an object is in the vicinity of this focused beam, it will feel an attractive force, commonly termed the gradient force, as it is proportional to the gradient of the electric field intensity [120–123]. Although the combination of a laser beam and objective can only form a stationary optical trap, relative motion of the trapped object within the sample chamber can be achieved by mounting the sample cell on a 3-axis translation stage or incorporating beam-shaping optics or scanning mirrors into the system. In the latter case, object motion is restricted to the field of view of the objective, while in the former case, the only limitation is the extent of the chamber or travel range of the stage.

OT are a versatile manipulation technique, as they can be used to trap and assemble a variety of objects with different shapes, sizes, and material compositions, including dielectric microspheres [99, 101, 102, 106, 125, 127, 128], metallic nanoparticles [126, 129] nanowires, [110, 130–135], and biological media [104, 124, 136–139]. While OT can effectively position a diverse array of objects in 3D, it is necessary to immobilize these objects in the absence of the optical trap to form self-standing structures. This has been achieved using several approaches, including biochemical binding [101, 125, 128, 132, 140], colloidal engineering [102, 129], and photopolymerization [98, 103, 141].

Many studies have demonstrated the potential of OT as a micro and nanoassembly platform (Figure 8). Mirsaidov et al. fabricated arrays of *Escherichia coli* cells to demonstrate the potential of OT in the field of tissue engineering, as OT can manipulate live cells without significantly affecting cell viability [124]. Melzer et al. created a 3D simple cubic lattice with alternating 1 μm polystyrene spheres of biotin and streptavidin functionalization, demonstrating the 3D and multimaterial capabilities of OT [125]. In this study, the large lateral translation range of the stage (~2 cm) and fast writing speed enabled by a high laser power allows the fabrication of extended structures out of a relatively large number of building blocks. Benito et al. constructed a 3-layer face-centered cubic lattice with an integrated line defect composed of 3 μm polystyrene spheres, relying on the depletion force to mediate binding [102].

At the nanoscale, fabrication using OT has so far received less attention than at the microscale. However, there are a few examples, including the trapping and positioning of ~40 nm gold nanoparticles on a substrate,
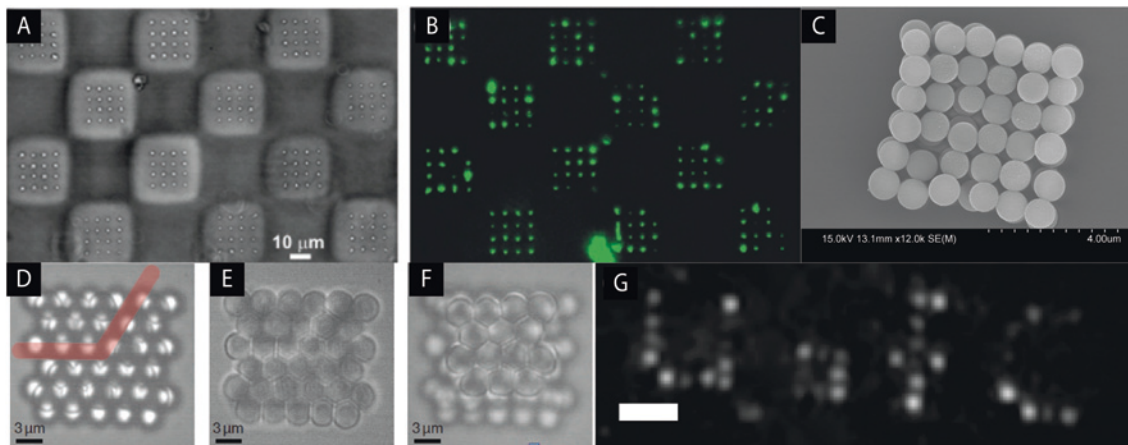
Figure 8: Micro and nanofabrication using OT. (A–B) Arrays of *E. coli* assembled using OT and photopolymerization. After 5 h, 83% of cells are still viable, as determined from fluorescence imaging in (B). Reprinted with permission from Ref. [124]. (C) Two-layer simple cubic lattice consisting of alternating biotin- and avidin-coated 1 μm polystyrene spheres [125]. (D–F) Three-layer face centered cubic crystal assembly with line defect composed of 3 μm polystyrene spheres. Reprinted with permission from Ref. [102]. (G) Dark field microscope image of patterned "U of C" using ~40 nm gold nanoparticles. Reprinted with permission from Ref. [126].

exhibiting the size and material flexibility of the OT assembly platform [126]. Another nanoscale application is the assembly of optical waveguides (Figure 9). Li et al. used OT to trap and manipulate zinc oxide (ZnO) nanowires and immobilize them by subsequently melting a polymer film on the substrate. The ZnO nanowires successfully guided a beam from a green laser diode through a coupled arrangement of nanowires [110]. Barroso et al. used zeolite L crystals to guide a 532 nm laser beam. The crystal was manipulated at multiple locations using holographic OT,

Figure 9: Optical waveguides assembled using optical tweezers. (A–C) Optical microscope images of a zeolite L crystal guiding a 532 nm laser. As the zeolite L crystal is rotated, the output light is redirected parallel to the crystal axis. Reprinted with permission from Ref. [142]. (D–E) Assembled structure consisting of ZnO nanowires. A light source illuminates the structure at point 1 and propagates through the nanowires to point 2, as shown in (E). Reprinted with permission from Ref. [110].

permitting the controlled rotation of the crystal and redirection of the guided beam [142].

The main parameters influencing the ability of OT to efficiently fabricate 3D nanostructures include laser trapping power, lateral translation speeds, and positioning accuracy. The trapping power and translation speeds are inherently related quantities, as a stronger optical beam generally induces a stronger optical force on the trapped object [120, 143]. However, it is important to note that significant increases in power can lead to increases in laser absorption and heating, thereby destabilizing the optical trap and negating any enhancement in optical trapping force. For the case of nanoscale building blocks, specifically 100 nm diameter gold spheres, the current record for lateral manipulation speed is 150 μm/s, which was achieved with a ~150 mW trapping beam [143]. The achieved speed represents a fundamental limit imposed by heating effects at higher trapping powers. We also report the best positioning accuracy found in the literature for an OT assembly process of 50 nm for the manipulation of 1 μm polystyrene spheres [125]. Finally, we note that techniques to parallelize the optical trapping of multiple objects, such as time-sharing approaches (e.g. using scanning galvonometer mirrors) or beam shaping approaches (e.g. using a spatial light modulator), are effective ways to greatly improve the throughput of an OT assembly system [98, 144–146].
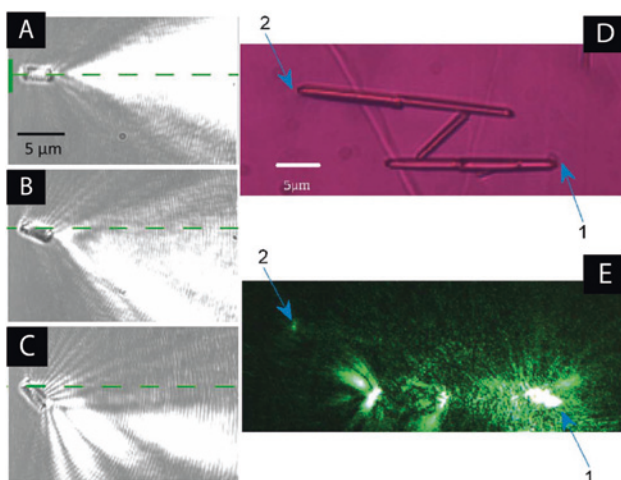
4 Inkjet printing

Inkjet printing encompasses a variety of nozzle-based methods such as electrospinning [147, 148], direct ink

writing (DIW) [20, 149, 150], and electrohydrodynamic printing (EHDP) [151–156]. Here we focus exclusively on DIW and EHDP, as these two methods are the most promising for micro and nanoscale fabrication. The electrospinning process, while it can produce high aspect ratio fibers with nanometer dimension, is primarily limited to polymers and has insufficient control in order to fabricate precise 3D geometries.

EHDP is a technique with many similarities to electrospinning that offers additional control over structure patterning. In the case of electrospinning, a large voltage on the order of tens of kilovolts is applied to the nozzle (while the substrate remains grounded), creating an electrostatic force on the polymer solution at the nozzle tip. In the absence of an applied voltage, the primary force felt by the polymer solution is surface tension. The electrostatic force tends to oppose the surface tension, so when the voltage is sufficiently large, a jet of solution will discharge from the nozzle [147]. As the discharged solution travels through the air to the substrate, it elongates, forming a polymer fiber on the substrate as the solvent evaporates. This is advantageous, as it allows for the printing of structures with feature sizes below that of the printing nozzle. However, in conventional electrospinning, the distance between the nozzle and substrate is several centimeters, limiting control over structure design. In contrast, EHDP uses a reduced nozzle-substrate distance and reduced voltages, on the order of hundreds of microns and hundreds of volts, respectively [148]. Additionally, applying a pulsed voltage signal allows for the fabrication of structures from discrete droplets of solution, often referred to as drop-on-demand [148, 157].

The drop-on-demand mode of printing enables the fabrication of complex 3D micro- and nano-structures.

The main distinction between EHDP and DIW is that no bias voltage is applied between the nozzle and substrate in the DIW process. DIW uses multiple methods in order to extrude ink through the nozzle, such as microfluidic print heads [158] and piezoelectric print heads [159]. In the case of microfluidic print heads, a microfluidic pump provides the necessary pressure to push ink through the nozzle. For a piezoelectric print head, electrical impulses sent to a piezoelectric actuator will force ink to be ejected through the nozzle. In either case, DIW resolution is typically comparable to the nozzle diameter, restricting feature sizes of this technique to around one micron [160]. Nevertheless, DIW has excellent material compatibility and has been demonstrated with a wide array of materials including metals [150, 161–164], ceramics [165–167], polymers [160, 168, 169], and even biological media [170, 171].

Unlike DIW, EHDP has demonstrated feature sizes down to ~50 nm using a colloidal gold dispersion and 1 μm nozzle diameter, achieved through a detailed analysis of ink formulation, bias voltage, and ejection event frequency [172]. In terms of process efficiency, there is typically a trade off between printing speed and minimum feature size. Methods to overcome this process limitation, however, include the use of multiple print heads in parallel or a combination of printing techniques, such as DIW to print larger-scale structures and EHDP for high-resolution features [153].

Figure 10 demonstrates the potential of inkjet printing as a versatile 3D nanofabrication technique. Several studies have investigated the minimum achievable feature size and 3D capability of the inkjet printing platform [128, 172–176].
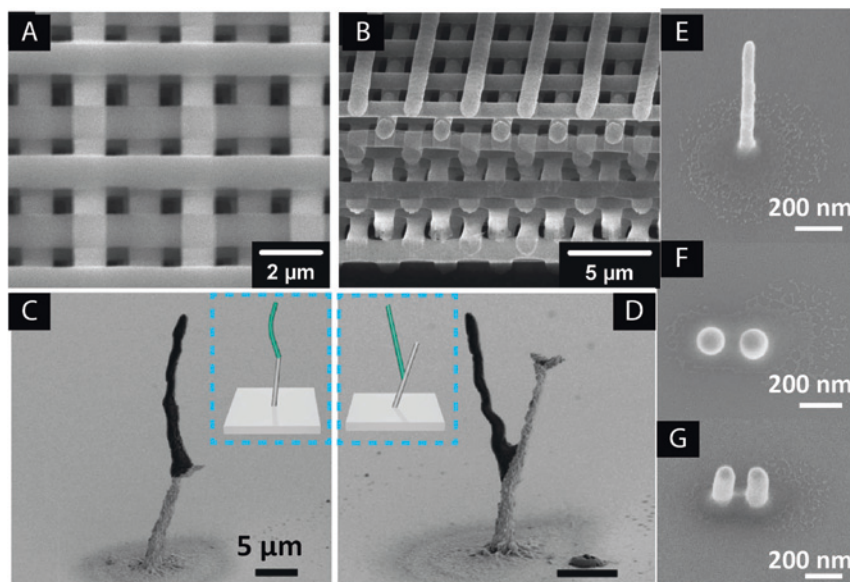

Figure 10: 3D micro and nanostructures fabricated using inkjet printing. (A–B) SEM images of polymer woodpile structures with 1 μm diameter rods and center-to-center rod spacing of 4 μm. Reprinted with permission from Ref. [160]. (C–D) SEM images of heterogeneous pillars printed with black and white pillars made of anthracene and silver, respectively. Reprinted with permission from [174]. (E–G) SEM images of nanopillars of gold printed using EHDP. Reprinted with permission from [172].

Galliker et al. printed gold nanopillars with diameter around 50 nm and aspect ratio of 17 using a nozzle diameter of 1 μm [172]. Gratson et al. printed a 16-layer woodpile structure with 1 μm feature size using a 1 μm nozzle [160]. An et al. printed heterogeneous pillar structures using silver and anthracence inks, demonstrating the ability to form a single structure using multiple materials [174].

In the following sections, we describe various applications of inkjet printing including the printing of photonic crystals (PCs), optical waveguides, and LEDs.

4.1 Photonic crystals

There are two types of PC structures that are typically fabricated using inkjet printing methods. In the first case, the PC lattice is directly written using the printer [149], as demonstrated in Figure 11. Gratson et al. used a polymer ink composed of polyethylenimine and polyacrilic acid and 1 μm diameter glass nozzle to form a woodpile structure *via* DIW [160]. Wang et al. used a TiO$_2$ sol-gel ink and 60 μm nozzle in order to create woodpile PCs operating in the terahertz frequency range [165]. Zhu et al. fabricated woodpile PCs for application at terahertz frequencies, but used a barium titanate (BaTiO$_3$) ink embedded in PDMS, with nozzle diameter of 180 μm [166].

In the second case, the ink contains colloidal particles which form the PC lattice [179], demonstrated in Figure 12. For these structures, the colloidal particles will self-assemble upon drying to form a structure consisting of close-packed spheres. Shen et al. fabricated a biosensor using Y-shaped PC channels which also aid in fluidic transport [178]. The PC channels were written using a colloidal ink consisting of core–shell nanoparticles with a polystyrene core and a shell made of polymethylmethacrylate (PMMA) and polyacrlic acid. Each PC channel has a different structural color and the shift of the biofunctionalized PC reflectance spectrum effectively determined the presence of desired biomarkers. Park et al. fabricated colloidal PC microarrays by placing ink droplets containing polystyrene nanospheres, which form structured hemispherical assemblies [177].

4.2 Optical waveguides

There are many examples of planar waveguides fabricated using inkjet methods, shown in Figure 13. Lorang et al. used a core–shell ink with a photocurable liquid core to print a network of optical waveguides [180]. The network effectively guides light with minimal cross-talk,
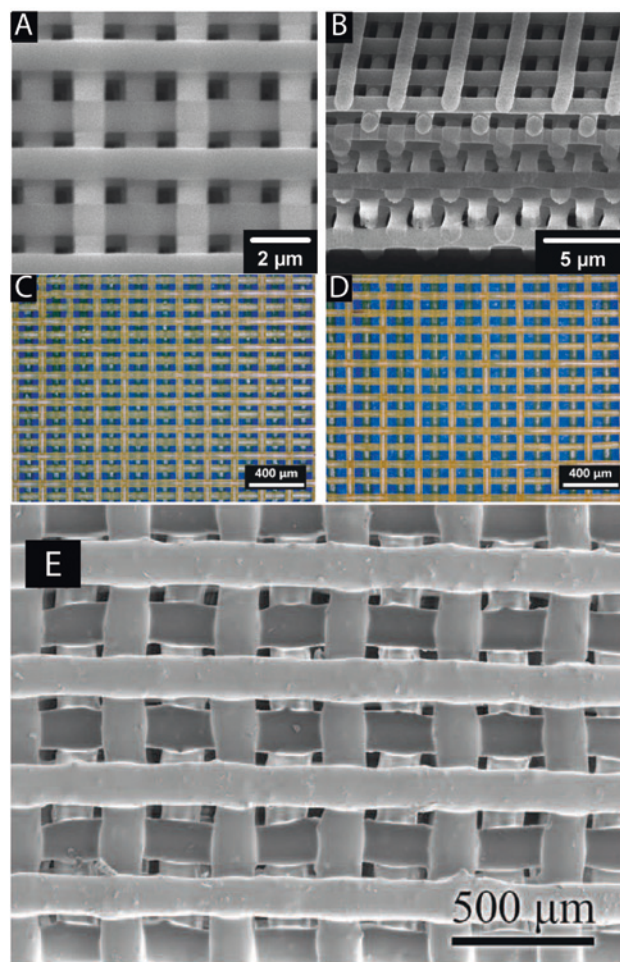
Figure 11: 3D woodpile photonic crystal structures written using DIW. (A–B) SEM images of polymer woodpile structure with 1 μm diameter rods and center-to-center rod spacing of 4 μm. Reprinted with permission from Ref. [160]. (C–D) Optical images of sol-gel titanium dioxide (TiO$_2$) woodpile structures with varying lattice periods of 200 μm (C) and 250 μm (D). Reprinted with permission from Ref. [165]. (E) SEM image of woodpile structure written using 40 wt% BaTiO$_3$/PDMS composite ink and a 180 μm nozzle. Reprinted with permission from Ref. [166].

as demonstrated in Figure 13A. Zhang et al. printed a waveguide-coupled microring resonator, as well as two coupled microring resonators by printing solvent droplets on a thin polystyrene film [181]. The former structure is shown in Figure 13B. The solvent causes the film to dissolve locally and form a microstructure under the surface tension of the droplets, achieving waveguide diameters around 5 μm. Shining a beam of light on to the resonator leads to coupling of the light into the waveguide, demonstrating the good optical quality of the deposited structures. Lastly, Parker et al. printed silk waveguides with 5 μm cross section that successfully guided visible light [169].
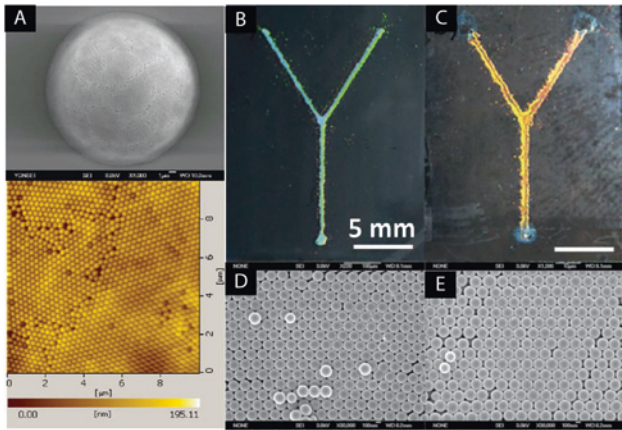
Figure 12: Photonic crystals formed using colloidal inks. (A) Photonic crystal droplet containing 190 nm polystyrene particles. The top image is taken in the SEM while the bottom image is obtained using AFM. Reprinted with permission from Ref. [177]. (B–E) PC microfluidic channels written using multiple inks with different colloidal particle sizes for application as a biosensor. Reprinted with permission from Ref. [178]: (B–C) different microfluidic Y-channels written using different colloidal inks and exhibiting varied structural color due to colloidal particle size; (D–E) top-view SEM images of the channels with 216 nm (D) and 235 nm (E) colloidal particles.

4.3 Light emitting diodes

Inkjet printing has been used for the printing of quantum dot (QD) based LEDs, or QLEDs (Figure 14). Kim et al. developed red and green QD inks and printed various
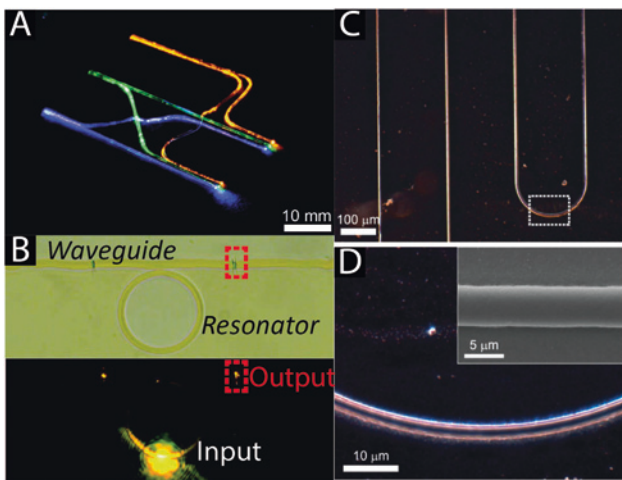

Figure 13: Optical waveguides written using inkjet printing. (A) Optical waveguide network with three LEDs, demonstrating the low crosstalk between waveguides. Reprinted with permission from Ref. [180]. (B) Microscope images of a microring resonator and a waveguide, demonstrating the guiding and coupling of the input laser beam. Reprinted with permission from Ref. [181]. (C-D) Images of a printed silk waveguide with SEM inset in (D). Reprinted with permission from Ref. [169].

patterns to demonstrate the versatility of EHDP [182]. They were able to print lines of QDs with lateral dimensions down to 250 nm. Yang et al. printed arrays of QDs with improved ink formulation, achieving minimal pixel diameters of 20 μm using DIW [184]. Kong et al. took QLED fabrication a step further by developing and printing the ink of all five layers of the structure, demonstrating the extensive material compatibility of DIW [183]. In this study, the researchers also demonstrated the ability of EHDP to print on non-planar surfaces. They printed the five layer QLED structure on a contact lens, illustrated in Figure 14E, which was first scanned in 3D to ensure conformal printing of the QLED layers.

5 Comparative discussion

We have discussed three classes of 3D nanofabrication techniques, namely laser induced transfer (LIT), light directed assembly (LDA), and inkjet printing (IP), which we believe are promising approaches for fabricating high-resolution, multimaterial structures in three dimensions. LIT has broad material compatibility and has achieved lateral feature sizes down to 70 nm and typical write speeds up to several mm/s. We note that a 70 nm feature size for LIT is not illustrated in Figure 1 since no writing speed is reported in the study [61]. In LDA, OT have similarly demonstrated the ability to manipulate multiple materials, and achieved 40 nm feature size in an assembly application with placement accuracy down to 50 nm and manipulation speeds up to ~200 μm/s. Direct ink writing, one technique of interest within the scope of IP, has demonstrated feature sizes down to 1 μm and fast writing speeds up to several mm/s. Finally, EHDP, another class of IP, has demonstrated feature sizes down to 50 nm and typical write speeds on the order of 100s of μm/s.

Although there are significant overlaps in the ranges of minimum lateral feature sizes and write speeds for each of these techniques, there are distinct practical advantages and disadvantages associated with each. In the case of LIT, a primary advantage is the ability to transfer building blocks of widely varying size and shape, as indicated by the range of feature sizes spanned in Figure 1. As building blocks can be generated from a continuous medium, their geometry can be specified using beam shaping or photomasks. Simultaneously utilizing large and small building blocks increases fabrication efficiency in multi-scale structures, like hierarchical materials. In addition, LIT boasts greater material diversity than either LDA or IP, owing to the ability to use either solid or liquid phase donor substrates, which can be prepared using broadly-
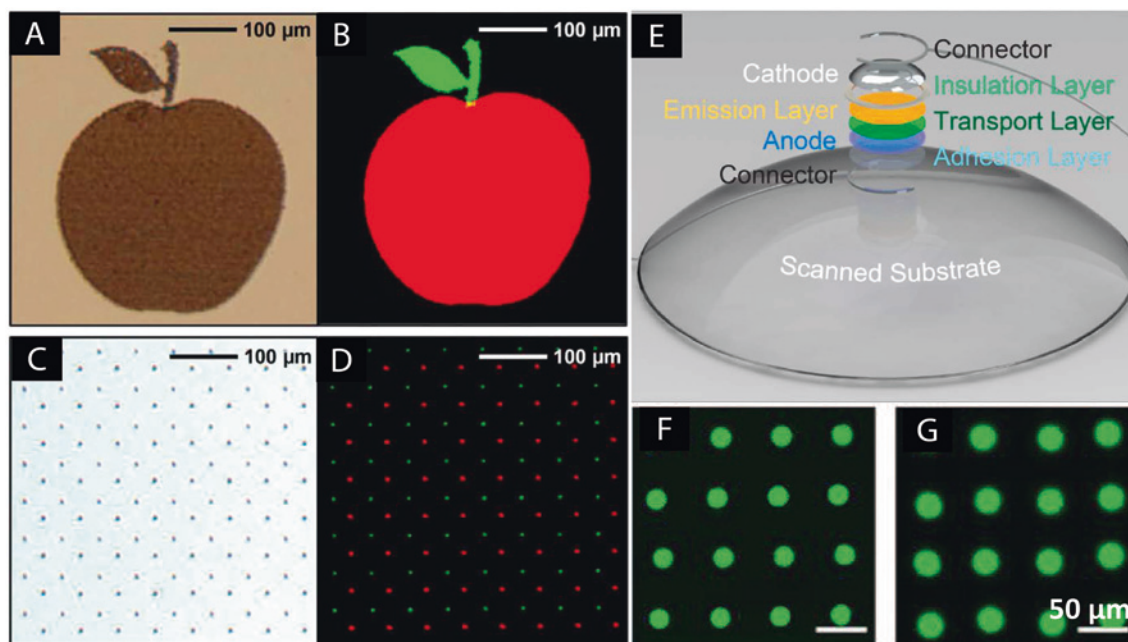
Figure 14: QD LEDs written using inkjet printing. (A–D) Varying patterns of QDs written on a substrate, demonstrating the high resolution and multi-material capability of the EHDP process. Optical image (A) and composite fluorescent image (B) of an apple printed using red and green QDs. Optical image (C) and composite fluorescent image (D) of arrays of red and green QDs printed using the drop on demand mode. Reprinted with permission from Ref. [182]. (E) Schematic of the 5-layer QD LED written using five distinct inks. The structure was printed on a curvilinear substrate, specifically a contact lens, in order to demonstrate conformal printing on nonflat substrates. Reprinted with permission from Ref. [183]. (F–G) Arrays of QDs with varying droplet size. Reprinted with permission from Ref. [184].

compatible and cost-effective film deposition procedures. Furthermore, in the solid phase, it is possible to prepare layered donor substrates, enabling the transfer of multi-layered building blocks using a single laser pulse. On the other hand, a disadvantage of solid-phase LIT is the frequent generation of debris and the potential destructive effect of the laser-induced shock wave with the transferred pixel. Although liquid-phase LIT can overcome these specific disadvantages, the donor substrate is subject to varying material properties over time due to solvent evaporation and it typically requires an additional post-processing step such as sintering to obtain the final fabricated device.

One advantage associated with LDA is the ability to incorporate building blocks with unique shapes and chemical properties. Chemically synthesized spheres, cubes, rings, rods, wires, platelets, and stars can all be optically manipulated. Furthermore, these building blocks can be fabricated with multiple materials, as in the case of core–shell nanoparticles. These building blocks could be used to fabricate photonic crystal and metamaterial structures with a specially designed unit cell basis. LDA is typically performed in an aqueous solution, making it more biocompatible than either LIT or IP. On the other hand, for many applications, the aqueous solution must be removed,

which can cause disruption due to surface tension. Additionally, the procedure for immobilizing the structure in solution as it is being assembled typically demands complex chemical or physical binding mechanisms. Finally, LDA has some fundamental restrictions on building block material and size combinations, as the fabrication method is predicated on the light-object interaction. As a simple example, the manipulation of metallic objects larger than 200 nm in 3D requires specialized laser beam shapes like bottle beams. In general, LDA is not particularly efficient for larger microscale building blocks, as evidenced by relative lack of LDA points in the right half of Figure 1.

Of the two types of IP reviewed here, DIW is best suited for printing microscale features, whereas EHDP is better suited for nanoscale features, as shown in Figure 1. A main advantage of IP methods is the ease of switching building block size on-the-fly, which can be achieved by varying the applied voltage duty cycle in EHDP. With a longer duration voltage pulse, more material is jetted from the nozzle, leading to a larger printed building block. Similar to LIT methods, this enables the efficient fabrication of hierarchical structures with a range of feature sizes. One disadvantage of IP is the technical challenge of creating new workable ink formulations for each desired material, as ink properties significantly affect the final properties of the

fabricated structure. Additionally, parallelization is inherently more difficult in inkjet printing methods, as it is more challenging to incorporate multiple printing nozzles than to multiplex a laser beam, which is the necessary step to parallelize LDA and LIT methods. Finally, for nanoscale feature sizes, EHDP tends to be slower than LIT and OT, as can be seen in Figure 1.

6 Conclusion

3D nanofabrication is an enabling technology for a variety of different fields and applications. Although these techniques have shown great potential thus far, we believe process efficiency improvements will be the most important next step in making these methods more widely adopted. In particular, high-quality complex structures composed of many discrete components will require 3D registration and alignment with nanometer-level repeatabilty while maintaining high write speeds, which is a technically challenging requirement. One route to increased write speeds is through the use of parallelization, using spatial light modulators or digital micromirror devices in the case of LIT or LDA, or multiple nozzles in the case of IP. Another route to increased fabrication speed is by incorporating widely varying, hierarchical discrete component feature sizes: large components can be used for filling large volumes and smaller components for areas requiring high resolution. As the LIT, LDA, and IP approaches develop, we expect a more rapid translation of these techniques from research labs into user-facility and manufacturing settings, ultimately leading to a major impact on the future of 3D nanoscale additive manufacturing.

References

[1] C. M. Soukoulis and M. Wegener, "Past achievements and future challenges in the development of three-dimensional photonic metamaterials," *Nat. Photon.*, vol. 5, pp. 523–530, 2011.

[2] J. K. Gansel, M. Thiel, M. S. Rill, et al., "Gold helix photonic metamaterial as broadband circular polarizer," *Science*, vol. 325, pp. 1513–1515, 2009.

[3] J. B. Pendry, D. Schurig, and D. R. Smith, "Controlling electromagnetic fields," *Science*, vol. 312, pp. 1780–1782, 2006.

[4] A. F. Koenderink, A. Alù, and A. Polman, "Nanophotonics: Shrinking light-based technology," *Science*, vol. 348, pp. 516–521, 2015.

[5] S. J. B. Yoo, B. Guan, and R. P. Scott, "Heterogeneous 2D/3D photonic integrated microsystems," *Microsyst. Nanoeng.*, 2, 1–9, 2016.

[6] Y. Zhang, Y. C. Ling, Y. Zhang, K. Shang, and S. J. B. Yoo, "High-density wafer-scale 3-D silicon-photonic integrated circuits," *IEEE J. Sel. Top. Quant. Electron.*, vol. 24, pp. 1–10, 2018.

[7] J. Langer, D. Jimenez de Aberasturi, J. Aizpurua, et al., "Present and future of surface-enhanced raman scattering," *ACS Nano*, vol. 14, pp. 28–117, 2020.

[8] M. D. Baaske, M. R. Foreman, and F. Vollmer, "Singlemolecule nucleic acid interactions monitored on a label-free microcavity biosensor platform," *Nat. Nanotechnol.*, vol. 9, pp. 933–939, 2014.

[9] C. Li, L. Chen, E. McLeod, and J. Su, "Dark mode plasmonic optical microcavity biochemical sensor," *Photon. Res.*, vol. 7, pp. 939–947, 2019.

[10] L. Chen, C. Li, Y. M. Liu, J. Su, and E. McLeod, "Simulating robust far-field coupling to traveling waves in large threedimensional nanostructured high-Q microresonators," *Photon. Res.*, vol. 7, pp. 967–976, 2019.

[11] S. Jayasuriya, S. Sivaramakrishnan, E. Chuang, D. Guruaribam, A. Wang, and A. Molnar, "Dual light field and polarization imaging using CMOS diffractive image sensors," *Opt. Lett.*, vol. 40, pp. 2433–2436, 2015.

[12] S. Yi, M. Zhou, Z. Yu, et al., "Subwavelength anglesensing photodetectors inspired by directional hearing in small animals," *Nat. Nanotechnol.*, vol. 13, pp. 1143–1147, 2018.

[13] L. Martinelli, H. Choumane, K. N. Ha, et al., "Sensorintegrated fluorescent microarray for ultrahigh sensitivity direct-imaging bioassays: Role of a high rejection of excitation light," *Appl. Phys. Lett.*, vol. 91, Art no. 083901, 2007.

[14] M. M. Shulaker, G. Hills, R. S. Park, et al., "Three-dimensional integration of nanotechnologies for computing and data storage on a single chip," *Nature*, vol. 547, pp. 74–78, 2017.

[15] Y. L. Zhang, Q. D. Chen, H. Xia, and H. B. Sun, "Designable 3D nanofabrication by femtosecond laser direct writing," *Nano Today*, vol. 5, pp. 435–448, 2010.

[16] H. B. Sun and S. Kawata, "Two-photon photopolymerization and 3D lithographic microfabrication," in *NMR • 3D Analysis • Photopolymerization*, Eds., N. Fatkullin, T. Ikehara, H. Jinnai et al., Apvances in Polymer Science (Springer Berlin Heidelberg, Berlin, Heidelberg, 2004), pp. 169–273, https://doi.org/10.1007/b94405.

[17] A. Camposeo, L. Persano, M. Farsari, and D. Pisignano, "Additive manufacturing: applications and directions in photonics and optoelectronics," *Adv. Opt. Mater.*, vol. 7, Art no. 1800419, 2019.

[18] Q. Li, D. Grojo, A. P. Alloncle, B. Chichkov, and P. Delaporte, "Digital laser micro- and nanoprinting," *Nanophotonics*, vol. 8, pp. 27–44, 2019.

[19] K. Sugioka and Y. Cheng, "Femtosecond laser threedimensional micro- and nanofabrication," *Appl. Phys. Rev.*, vol. 1, Art no. 041303, 2014.

[20] M. Mao, J. He, X. Li, et al., "The emerging frontiers and applications of high-resolution 3D printing," *Micromachines*, vol. 8, p. 113, 2017.

[21] K.-H. Leitz, Y.-C. Tsai, F. Flad, et al., "Multiphoton polymerization using optical trap assisted nanopatterning," *Appl. Phys. Lett.*, vol. 102, Art no. 243108, 2013.

[22] L. Jonušauskas, S. Juodkazis, and M. Malinauskas, "Optical 3D printing: bridging the gaps in the mesoscale," *J. Optic*, vol. 20, Art no. 053001, 2018.

[23] M. Grzelczak, J. Vermant, E. M. Furst, and L. M. Liz-Marzán, "Directed Self-Assembly of Nanoparticles," *ACS Nano*, vol. 4, pp. 3591–3605, 2010.

[24] E. McLeod, C. Nguyen, P. Huang, W. Luo, M. Veli, and A. Ozcan, "Tunable vapor-condensed nanolenses," *ACS Nano*, vol. 8, pp. 7340–7349, 2014.

[25] E. McLeod and A. Ozcan, "Nano-imaging enabled via selfassembly," *Nano Today*, vol. 9, pp. 560–573, 2014.

[26] Z. Göröcs, E. McLeod, and A. Ozcan, "Enhanced light collection in fluorescence microscopy using self-assembled microreflectors," *Sci. Rep.*, vol. 5, 2015, https://doi.org/10.1038/srep10999.

[27] P. Delaporte and A. P. Alloncle, "Laser-induced forward transfer: A high resolution additive manufacturing technology," *Optic Laser. Technol. The year Light: Opt. Fiber Sensors Laser Mater. Process.*, vol. 78, pp. 33–41, 2016.

[28] A. Piqué, R. C. Y. Auyeung, H. Kim, N. A. Charipar, and S. A. Mathews, "Laser 3D micro-manufacturing," *J. Phys. D: Appl. Phys.*, vol. 49, Art no. 223001, 2016.

[29] A. Piqué and P. Serra, *Laser Printing of Functional Materials: 3D Microfabrication, Electronics and Biomedicine*, Wiley, 2018, https://doi.org/10.1002/9783527805105.

[30] M. S. Brown, C. F. Brasz, Y. Ventikos, and C. B. Arnold, "Impulsively actuated jets from thin liquid films for high-resolution printing applications," *J. Fluid. Mech.*, vol. 709, pp. 341–370, 2012.

[31] S. Papazoglou and I. Zergioti, "Laser Induced Forward Transfer (LIFT) of nano-micro patterns for sensor applications," *Microelectron. Eng.*, vol. 182, pp. 25–34, 2017.

[32] D. Munoz-Martin, C. F. Brasz, Y. Chen, M. Morales, C. B. Arnold, and C. Molpeceres, "Laser-induced forward transfer of high-viscosity silver pastes," *Appl. Surf. Sci.*, vol. 366, pp. 389–396, 2016.

[33] Q. Li, A. P. Alloncle, D. Grojo, and P. Delaporte, "Laserinduced nano-jetting behaviors of liquid metals," *Appl. Phys. A.*, vol. 123, p. 718, 2017.

[34] P. Serra and A. Piqué, "Laser-induced forward transfer: fundamentals and applications," *Adv. Mater. Technol.*, vol. 4, Art no. 1800099, 2019.

[35] R. Fardel, M. Nagel, F. Nüesch, T. Lippert, and A. Wokaun, "Shadowgraphy investigation of laser-induced forward transfer: Front side and back side ablation of the triazene polymer sacrificial layer," *Appl. Surf. Sci. Laser Plasma Micro- and Nano-Scale Mater. Process. Diagn.*, vol. 255, pp. 5430–5434, 2009.

[36] N. T. Kattamis, N. D. McDaniel, S. Bernhard, and C. B. Arnold, "Laser direct write printing of sensitive and robust light emitting organic molecules," *Appl. Phys. Lett.*, vol. 94, Art no. 103306, 2009.

[37] M. S. Brown, N. T. Kattamis, and C. B. Arnold, "Timeresolved study of polyimide absorption layers for blisteractuated laser-induced forward transfer," *J. Appl. Phys.*, vol. 107, Art no. 083103, 2010.

[38] E. Turkoz, A. Perazzo, H. Kim, H. A. Stone, and C. B. Arnold, "Impulsively induced jets from viscoelastic films for high- resolution printing," *Phys. Rev. Lett.*, vol. 120, Art no. 074501, 2018.

[39] S. A. Mathews, R. C. Y. Auyeung, H. Kim, N. A. Charipar, and A. Piqué, "High-speed video study of laser-induced forward transfer of silver nano-suspensions," *J. Appl. Phys.*, vol. 114, Art no. 064910, 2013.

[40] J. Wang, R. C. Y. Auyeung, H. Kim, N. A. Charipar, and A. Piqué, "Three-dimensional printing of interconnects by laser direct-write of silver nanopastes," *Adv. Mater.*, vol. 22, pp. 4462–4466, 2010.

[41] R. Fardel, M. Nagel, F. Nüesch, T. Lippert, and A. Wokaun, "Laser-induced forward transfer of organic LED building blocks studied by time-resolved shadowgraphy," *J. Phys. Chem. C*, vol. 114, pp. 5617–5636, 2010.

[42] M. Zenou, A. Sa'ar, and Z. Kotler, "Laser transfer of metals and metal alloys for digital microfabrication of 3D objects," *Small*, vol. 11, pp. 4082–4089, 2015.

[43] Q. Li, A. P. Alloncle, D. Grojo, and P. Delaporte, "Generating liquid nanojets from copper by dual laser irradiation for ultrahigh resolution printing," *Optics Express*, vol. 25, pp. 24164–24172, 2017.

[44] A. I. Kuznetsov, A. B. Evlyukhin, C. Reinhardt, et al., "Laserinduced transfer of metallic nanodroplets for plasmonics and metamaterial applications," *J. Opt. Soc. Am. B.*, vol. 26, p. B130, 2009.

[45] D. M. Zhigunov, A. B. Evlyukhin, A. S. Shalin, U. Zywietz, and B. N. Chichkov, "Femtosecond laser printing of single Ge and SiGe nanoparticles with electric and magnetic optical resonances," *ACS Photonics*, vol. 5, pp. 977–983, 2018.

[46] M. Feinaeugle, R. Pohl, T. Bor, T. Vaneker, and G. w. Römer, "Printing of complex free-standing microstructures via laserinduced forward transfer (LIFT) of pure metal thin films," *Addit. Manuf.*, vol. 24, pp. 391–399, 2018.

[47] M. Zenou and Z. Kotler, "Printing of metallic 3D microobjects by laser induced forward transfer," *Optics Express*, vol. 24, p. 1431, 2016.

[48] M. Zenou, A. Sa'ar, and Z. Kotler, "Laser jetting of femtoliter metal droplets for high resolution 3D printed structures," *Sci. Rep.*, vol. 5, Art no. 17265, 2015.

[49] C. W. Visser, R. Pohl, C. Sun, G. W. Romer, B. H. i. t. Veld, and D. Lohse, "Toward 3D printing of pure metals by laser- induced forward transfer," *Adv. Mater.*, vol. 27, pp. 4087–4092, 2015.

[50] C. L. Sones, K. S. Kaur, P. Ganguly, et al., "Laser-induced-forward-transfer: a rapid prototyping tool for fabrication of photonic devices," *Appl. Phys. A*, vol. 101, pp. 333–338, 2010.

[51] C. Florian, S. Piazza, A. Diaspro, P. Serra, and M. Duocastella, "Direct laser printing of tailored polymeric microlenses," *ACS Appl. Mater. Interfaces*, vol. 8, pp. 17028–17032, 2016.

[52] A. Palla-Papavlu, V. Dinca, I. Paraico, et al., "Microfabrication of polystyrene microbead arrays by laser induced forward transfer," *J. Appl. Phys.*, vol. 108, Art no. 033111, 2010.

[53] J. M. P. Almeida, K. T. Paula, C. B. Arnold, and C. R. Mendonça, "Sub-wavelength self-organization of chalcogenide glass by direct laser writing," *Opt. Mater.*, vol. 84, pp. 259–262, 2018.

[54] M. Feinaeugle, C. L. Sones, E. Koukharenko, B. Gholipour, D. W. Hewak, and R. W. Eason, "Laser-induced forward transfer of intact chalcogenide thin films: resultant morphology and thermoelectric properties," *Appl. Phys. A*, vol. 112, pp. 1073–1079, 2013.

[55] T. Mattle, A. Hintennach, T. Lippert, and A. Wokaun, "Laser induced forward transfer of SnO2 for sensing applications using different precursors systems," *Appl. Phys. A*, vol. 110, pp. 309–316, 2013.

[56] A. Palla Papavlu, T. Mattle, S. Temmel, et al., "Highly sensitive SnO$_2$ sensor via reactive laser-induced transfer," *Sci. Rep.*, vol. 6, Art no. 25144, 2016.

[57] F. Guillemot, A. Souquet, S. Catros, et al., "High-throughput laser printing of cells and biomaterials for tissue engineering," *Acta Biomater.*, vol. 6, pp. 2494–2500, 2010.

[58] B. Hopp, T. Smausz, G. Szabó, et al., "Femtosecond laser printing of living cells using absorbing film-assisted laser-induced forward transfer," *Opt. Eng.*, vol. 51, Art no. 014302, 2012.

[59] M. Duocastella, M. Colina, J. M. Fernández-Pradas, P. Serra, and J. L. Morenza, "Study of the laser-induced forward transfer of liquids for laser bioprinting," *Appl. Surf. Sci. Photon-Assist. Synth. Process. Funct. Mater.*, vol. 253, pp. 7855–7859, 2007.

[60] U. Zywietz, A. B. Evlyukhin, C. Reinhardt, and B. N. Chichkov, "Laser printing of silicon nanoparticles with resonant optical electric and magnetic responses," *Nat. Commun.*, vol. 5, p. 3402, 2014.

[61] V. Sametoglu, V. T. K. Sauer, and Y. Y. Tsui, "Production of 70-nm Cr dots by laser-induced forward transfer," *Optics Express*, vol. 21, pp. 18525–18531, 2013.

[62] U. Zywietz, C. Reinhardt, A. B. Evlyukhin, T. Birr, and B. N. Chichkov, "Generation and patterning of Si nanoparticles by femtosecond laser pulses," *Appl. Phys. A*, vol. 114, pp. 45–50, 2014.

[63] D. P. Banks, C. Grivas, J. D. Mills, R. W. Eason, and I. Zergioti, "Nanodroplets deposited in microarrays by femtosecond Ti: sapphire laser-induced forward transfer," *Appl. Phys. Lett.*, vol. 89, Art no. 193107, 2006.

[64] C. Boutopoulos, C. Pandis, K. Giannakopoulos, P. Pissis, and I. Zergioti, "Polymer/carbon nanotube composite patterns via laser induced forward transfer," *Appl. Phys. Lett.*, vol. 96, Art no. 041104, 2010.

[65] W. T. Chen, M. L. Tseng, C. Y. Liao, et al., "Fabrication of three-dimensional plasmonic cavity by femtosecond laser-induced forward transfer," *Optics Express*, vol. 21, 618–625, 2013.

[66] S. H. Ko, H. Pan, S. G. Ryu, N. Misra, C. P. Grigoropoulos, and H. K. Park, "Nanomaterial enabled laser transfer for organic light emitting material direct writing," *Appl. Phys. Lett.*, vol. 93, Art no. 151110, 2008.

[67] J. Luo, R. Pohl, L. Qi, et al., "Printing functional 3D microdevices by Laser- induced forward transfer," *Small*, vol. 13, Art no. 1602553, 2017.

[68] A. Narazaki, T. Sato, R. Kurosaki, Y. Kawaguchi, and H. Niino, "Nano- and microdot array formation by laser-induced dot transfer," *Appl. Surf. Sci., Proc. Sixth Int. Conf. Photo-Excited Process. Appl.* 255, pp. 9703–9706, 2009.

[69] P. Serra, M. Colina, J. M. Fernández-Pradas, L. Sevilla, and J. L. Morenza, "Preparation of functional DNA microarrays through laser-induced forward transfer," *Appl. Phys. Lett.*, vol. 85, pp. 1639–1641, 2004.

[70] M. L. Tseng, P. C. Wu, S. Sun, et al., "Fabrication of multilayer metamaterials by femtosecond laser-induced forward-transfer technique," *Laser Photon. Rev.*, vol. 6, pp. 702–707, 2012.

[71] D. A. Willis and V. Grosu, "Microdroplet deposition by laserinduced forward transfer," *Appl. Phys. Lett.*, vol. 86, Art no. 244103, 2005.

[72] C. F. Brasz, J. H. Yang, and C. B. Arnold, "Tilting of adjacent laser-induced liquid jets," *Microfluid. Nanofluidics*, vol. 18, pp. 185–197, 2015.

[73] R. C. Y. Auyeung, H. Kim, S. Mathews, and A. Piqué, "Laser forward transfer using structured light," *Optics Express*, vol. 23, pp. 422–430, 2015.

[74] S. Surdo, R. Carzino, A. Diaspro, and M. Duocastella, "Single-shot laser additive manufacturing of high fill-factor microlens arrays," *Adv. Opt. Mater.*, vol. 6, Art no. 1701190, 2018.

[75] A. I. Aristov, U. Zywietz, A. B. Evlyukhin, C. Reinhardt, B. N. Chichkov, and A. V. Kabashin, "Laser-ablative engineering of phase singularities in plasmonic metamaterial arrays for biosensing applications," *Appl. Phys. Lett.*, vol. 104, Art no. 071101, 2014.

[76] M. L. Tseng, C. M. Chang, B. H. Chen, et al., "Fabrication of plasmonic devices using femtosecond laser-induced forward transfer technique," *Nanotechnology*, vol. 23, Art no. 444013, 2012.

[77] E. Y. Tiguntseva, G. P. Zograf, F. E. Komissarenko, et al., "Light-emitting Halide Perovskite nanoantennas," *Nano Lett.*, vol. 18, pp. 1185–1190, 2018.

[78] R. Fardel, M. Nagel, F. Nüesch, T. Lippert, and A. Wokaun, "Fabrication of organic light-emitting diode pixels by laserassisted forward transfer," *Appl. Phys. Lett.*, vol. 91, Art no. 061103, 2007.

[79] J. Shaw-Stewart, T. Lippert, M. Nagel, F. Nüesch, and A. Wokaun, "Laser-induced forward transfer of polymer light- emitting diode pixels with increased charge injection," *ACS Appl. Mater. Interfaces*, vol. 3, pp. 309–316, 2011.

[80] J. Shaw Stewart, T. Lippert, M. Nagel, F. Nüesch, and A. Wokaun, "Red-green-blue polymer light-emitting diode pixels printed by optimized laser-induced forward transfer," *Appl. Phys. Lett.*, vol. 100, Art no. 203303, 2012.

[81] J. Xu, J. Liu, D. Cui, M. Gerhold, A. Y. Wang, M. Nagel, and T. K. Lippert, "Laser-assisted forward transfer of multispectral nanocrystal quantum dot emitters," *Nanotechnology*, vol. 18, Art no. 025403, 2007.

[82] S. Zhang, Y. Zhai, R. Peng, et al., "Assembly of topographical micropatterns with optoelectronic tweezers," *Adv. Opt. Mater.*, vol. 7, Art no. 1900669, 2019.

[83] S. Zhang, N. Shakiba, Y. Chen, et al., "Patterned optoelectronic tweezers: a new scheme for selecting, moving, and storing dielectric particles and cells," *Small*, vol. 14, Art no. 1803342, 2018.

[84] A. Jamshidi, S. L. Neale, K. Yu, et al., "NanoPen: dynamic, low-power, and light-actuated patterning of nanoparticles," *Nano Lett.*, vol. 9, pp. 2921–2925, 2009.

[85] M. C. Wu, "Optoelectronic tweezers," *Nat. Photon.*, vol. 5, pp. 322–324, 2011.

[86] A. Kotnala and Y. Zheng, "Opto-thermophoretic fiber tweezers," *Nanophotonics*, vol. 8, pp. 475–485, 2019.

[87] L. Lin, X. Peng, M. Wang, et al., "Light-directed reversible assembly of plasmonic nanoparticles using plasmon- enhanced thermophoresis," *ACS Nano*, vol. 10, pp. 9659–9668, 2016.

[88] L. Lin, X. Peng, X. Wei, Z. Mao, C. Xie, and Y. Zheng, "Thermophoretic tweezers for low-power and versatile manipulation of biological cells," *ACS Nano*, vol. 11, pp. 3147–3154, 2017.

[89] L. Lin, J. Zhang, X. Peng, et al., "Opto-thermophoretic assembly of colloidal matter," *Sci. Adv.*, vol. 3, p. e1700458, 2017.

[90] X. Peng, J. Li, L. Lin, Y. Liu, and Y. Zheng, "Opto- thermophoretic manipulation and construction of colloidal superstructures in photocurable hydrogels," *ACS Appl. Nano Mater.*, vol. 1, pp. 3998–4004, 2018.

[91] N. Harris, M. J. Ford, M. B. Cortie, and A. M. McDonagh, "Laser-induced assembly of gold nanoparticles into colloidal crystals," *Nanotechnology*, vol. 18, Art no. 365301, 2007.

[92] J. Li, L. Lin, Y. Inoue, and Y. Zheng, "Opto-thermophoretic tweezers and assembly," *J. Micro Nano- Manufacturing*, vol. 6, Art no. 040801, 2018.

[93] L. Lin, X. Peng, Z. Mao, W. Li, et al., "Bubble-pen lithography," *Nano Lett.*, vol. 16, pp. 701–708, 2016.

[94] B. Bangalore Rajeeva, L. Lin, E. P. Perillo, et al., "High-resolution bubble printing of quantum dots," *ACS Appl. Mater. Interfaces*, vol. 9, pp. 16725–16733, 2017.

[95] N. Armon, E. Greenberg, M. Layani, Y. S. Rosen, S. Magdassi, and H. Shpaisman, "Continuous nanoparticle assembly by a modulated photo-induced microbubble for fabrication of micrometric conductive patterns," *ACS Appl. Mater. Interfaces*, vol. 9, pp. 44214–44221, 2017.

[96] Y. Xie and C. Zhao, "An optothermally generated surface bubble and its applications," *Nanoscale*, vol. 9, pp. 6622–6631, 2017.

[97] H. Misawa, K. Sasaki, M. Koshioka, N. Kitamura, and H. Masuhara, "Laser manipulation and assembling of polymer latex particles in solution," *Macromolecules*, vol. 26, pp. 282–286, 1993.

[98] L. A. Shaw, S. Chizari, R. M. Panas, M. Shusteff, C. M. Spadaccini, and J. B. Hopkins, "Holographic optical assembly and photopolymerized joining of planar microspheres," *Opt. Lett.*, vol. 41, p. 3571, 2016.

[99] A. Ostendorf, R. Ghadiri, and S. I. Ksouri, "Optical tweezers in microassembly," *Proc. SPIE*, vol. 8607, 86070U, 2013, https://doi.org/10.1117/12.2006127.

[100] O. M. Maragò, P. H. Jones, P. G. Gucciardi, G. Volpe, and A. C. Ferrari, "Optical trapping and manipulation of nanostructures," *Nat. Nanotechnol.*, vol. 8, pp. 807–819, 2013.

[101] J. Köhler, R. Ghadiri, S. I. Ksouri, E. L. Gurevich, and A. Ostendorf, "Optical tweezers as manufacturing and characterization tool in microfluidics," *Proc. SPIE*, vol. 9164, 91642F, 2014, https://doi.org/10.1117/12.2063080.

[102] D. Benito, D. Carberry, S. Simpson, et al., "Constructing 3D crystal templates for photonic band gap materials using holographic optical tweezers," *Optics Express*, vol. 16, Art no. 13005, 2008.

[103] F. Dawood, S. Qin, L. Li, E. Y. Lin, and J. T. Fourkas, "Simultaneous microscale optical manipulation, fabrication and immobilisation in aqueous media," *Chem. Sci.*, vol. 3, p. 2449, 2012.

[104] G. R. Kirkham, E. Britchford, T. Upton, et al., "Precision assembly of complex cellular microenvironments using holographic optical tweezers," *Sci. Rep.*, vol. 5, p. 8577, 2015.

[105] R. E. Holmlin, M. Schiavoni, C. Y. Chen, S. P. Smith, M. G. Prentiss, and G. M. Whitesides, "Light-driven microfabrication: assembly of multicomponent, three-dimensional structures by using optical tweezers," *Angew. Chem. Int. Ed.*, vol. 39, pp. 3503–3506, 2000.

[106] R. Ghadiri, T. Weigel, C. Esen, and A. Ostendorf, "Microassembly of complex and three-dimensional microstructures using holographic optical tweezers," *J. Micromech. Microeng.*, vol. 22, Art no. 065016, 2012.

[107] S. C. Chapin, V. Germain, and E. R. Dufresne, "Automated trapping, assembly, and sorting with holographic optical tweezers," *Optics Express*, vol. 14, pp. 13095–13100, 2006.

[108] Z. Yan, J. Sweet, J. E. Jureller, M. J. Guffey, M. Pelton, and N. F. Scherer, "Controlling the position and orientation of single silver nanowires on a surface using structured optical fields," *ACS Nano*, vol. 6, pp. 8144–8155, 2012.

[109] O. E. C. Gould, S. J. Box, C. E. Boott, et al., "Manipulation and deposition of complex, functional block copolymer nanostructures using optical tweezers," *ACS Nano*, vol. 13, pp. 3858–3866, 2019.

[110] J. Li and G. Du, "Manipulation and assembly of ZnO nanowires with single holographic optical tweezers system," *Appl. Opt.*, vol. 53, p. 351, 2014.

[111] T. Yu, F. C. Cheong, and C. H. Sow, "The manipulation and assembly of CuO nanorods with line optical tweezers," *Nanotechnology*, vol. 15, pp. 1732–1736, 2004.

[112] Z. Chen, F. Nan, and Z. Yan, "Making permanent optical matter of plasmonic nanoparticles by in situ photopolymerization," *J. Phys. Chem. C*, vol. 124, pp. 4215–4220, 2020.

[113] Y. Montelongo, A. K. Yetisen, H. Butt, and S.-H. Yun, "Reconfigurable optical assembly of nanostructures," *Nat. Commun.*, vol. 7, Art no. 12002, 2016.

[114] F. Nan and Z. Yan, "Silver-nanowire-based interferometric optical tweezers for enhanced optical trapping and binding of nanoparticles," *Adv. Funct. Mater.*, vol. 29, Art no. 1808258, 2019.

[115] Y. Liu, L. Lin, B. Bangalore Rajeeva, et al., "Nanoradiator-mediated deterministic opto- thermoelectric manipulation," *ACS Nano*, vol. 12, pp. 10383–10392, 2018.

[116] J. T. Bahns, S. K. R. S. Sankaranarayanan, S. K. Gray, and L. Chen, "Optically directed assembly of continuous mesoscale filaments," *Phys. Rev. Lett.*, vol. 106, Art no. 095501, 2011.

[117] N.-D. Dinh, R. Luo, M. T. A. Christine, et al., "Effective light directed assembly of building blocks with microscale control," *Small*, vol. 13, Art no. 1700684, 2017.

[118] J. Li, E. H. Hill, L. Lin, and Y. Zheng, "Optical nanoprinting of colloidal particles and functional structures," *ACS Nano*, vol. 13, pp. 3783–3795, 2019.

[119] J. Li, Y. Liu, L. Lin, et al., "Optical nanomanipulation on solid substrates via optothermally-gated photon nudging," *Nat. Commun.*, vol. 10, p. 5672, 2019.

[120] A. Ashkin, "Forces of a single-beam gradient laser trap on a dielectric sphere in the ray optics regime," *Biophys. J.*, vol. 61, pp. 569–582, 1992.

[121] T. A. Nieminen, N. du Preez-Wilkinson, A. B. Stilgoe, V. L. Loke, A. A. Bui, and H. Rubinsztein-Dunlop, "Optical tweezers: theory and modelling," *J. Quant. Spectrosc. Radiat. Transf.*, vol. 146, pp. 59–80, 2014.

[122] D. G. Grier, "A revolution in optical manipulation," *Nature*, vol. 424, pp. 810–816, 2003.

[123] R. W. Bowman and M. J. Padgett, "Optical trapping and binding," *Rep. Prog. Phys.*, vol. 76, Art no. 026401, 2013.

[124] U. Mirsaidov, J. Scrimgeour, W. Timp, et al., "Live cell lithography: using optical tweezers to create synthetic tissue," *Lab Chip*, vol. 8, p. 2174, 2008.

[125] J. E. Melzer and E. McLeod, "Optical tweezers for micro- and nano-assembly," *Proc. SPIE*, vol. 11292, 1129209, 2020, https://doi.org/10.1117/12.2543241.

[126] M. J. Guffey and N. F. Scherer, "All-optical patterning of au nanoparticles on surfaces using optical traps," *Nano Lett.*, vol. 10, pp. 4302–4308, 2010.

[127] J. Köhler, R. Ghadiri, S. I. Ksouri, Q. Guo, E. L. Gurevich, and A. Ostendorf, "Generation of microfluidic flow using an optically

assembled and magnetically driven microrotor," *J. Phys. D. Appl. Phys.*, vol. 47, Art no. 505501, 2014.

[128] I. Y. Park, S. Y. Sung, J. H. Lee, and Y. G. Lee, "Manufacturing micro-scale structures by an optical tweezers system controlled by five finger tips," *J. Micromech. Microeng.*, vol. 17, pp. N82–N89, 2007.

[129] J. P. Hoogenboom, D. L. J. Vossen, C. Faivre-Moskalenko, M. Dogterom, and A. van Blaaderen, "Patterning surfaces with colloidal particles using optical tweezers," *Appl. Phys. Lett.*, vol. 80, pp. 4828–4830, 2002.

[130] S. W. Lee, G. Jo, T. Lee, and Y. G. Lee, "Controlled assembly of In_2O_3 nanowires on electronic circuits using scanning optical tweezers," *Optics Express*, vol. 17, Art no. 17491, 2009.

[131] Z. Yan, J. E. Jureller, J. Sweet, M. J. Guffey, M. Pelton, and N. F. Scherer, "Three-dimensional optical trapping and manipulation of single silver nanowires," *Nano Lett.*, vol. 12, pp. 5155–5161, 2012.

[132] L. Ikin, D. M. Carberry, J. A. Grieve, G. M. Gibson, M. J. Padgett, and M. J. Miles, "Construction and manipulation of structures using optical tweezers," *Proc. SPIE*, vol. 7038, 70380T, 2008, https://doi.org/10.1117/12.795109.

[133] R. Agarwal, K. Ladavac, Y. Roichman, G. Yu, C. M. Lieber, and D. G. Grier, "Manipulation and assembly of nanowires with holographic optical traps," *Optics Express*, vol. 13, p. 8906, 2005.

[134] P. J. Pauzauskie, A. Radenovic, E. Trepagnier, H. Shroff, P. Yang, and J. Liphardt, "Optical trapping and integration of semiconductor nanowire assemblies in water," *Nat. Mater.*, vol. 5, pp. 97–101, 2006.

[135] A. van der Horst, A. I. Campbell, L. K. van Vugt, D. A. M. Vanmaekelbergh, M. Dogterom, and A. v. Blaaderen, "Manipulating metal-oxide nanowires using counter-propagating optical line tweezers," *Optics Express*, vol. 15, Art no. 11629, 2007.

[136] Y. Wu, D. Sun, W. Huang, and N. Xi, "Dynamics analysis and motion planning for automated cell transportation with optical tweezers," *IEEE/ASME Trans. Mechatron.*, vol. 18, pp. 706–713, 2013.

[137] A. Barroso, S. Landwerth, M. Woerdemann, et al., "Optical assembly of bio-hybrid micro-robots," *Biomed. Microdevices*, vol. 17, p. 26, 2015.

[138] R. W. J. Applegate, J. Squier, T. Vestad, J. Oakey, and D. W. M. Marr, "Optical trapping, manipulation, and sorting of cells and colloids in microfluidic systems with diode laser bars," *Optics Express*, vol. 12, pp. 4390–4398, 2004.

[139] Bin Cao, L. Kelbauskas, S. Chan, R. M. Shetty, D. Smith, and D. R. Meldrum, "Rotation of single live mammalian cells using dynamic holographic optical tweezers," *Optic Laser. Eng.*, vol. 92, pp. 70–75, 2017.

[140] K. Castelino, S. Satyanarayana, and M. Sitti, "Manufacturing of two and three-dimensional micro/nanostructures by integrating optical tweezers with chemical assembly," *Robotica*, vol. 23, pp. 435–439, 2005.

[141] J. T. Fourkas, F. Dawood, S. Qin, L. Li, et al., "Creation of multimaterial micro- and nanostructures through aqueous-based fabrication, manipulation, and immobilization," *Proc. SPIE*, vol. 8970, 89700M, 2014, https://doi.org/10.1117/12.2042545.

[142] A. Barroso, K. Dieckmann, C. Alpmann, T. Buscher, A. Studer, and C. Denz, "Nanoassembled dynamic optical waveguides and sensors based on zeolite L nanocontainers," *Proc. SPIE*,

vol. 9379, 93790U, 2015, https://doi.org/10.1117/12.2079156.

[143] J. E. Melzer and E. McLeod, "Fundamental limits of optical tweezer nanoparticle manipulation speeds," *ACS Nano*, vol. 12, pp. 2440–2447, 2018.

[144] R. Ghadiri, Q. Guo, I. Yeoh, C. Esen, and A. Ostendorf, "Process limitations in microassembling using holographic optical tweezers," *Proc. SPIE*, vol. 8244, 82440L, 2012, https://doi.org/10.1117/12.906679.

[145] D. Cojoc, "Dynamic multiple optical trapping by means of diffractive optical elements," *Microelectron. Eng.*, vol. 73–74, pp. 927–932, 2004.

[146] W. J. Hossack, E. Theofanidou, J. Crain, K. Heggarty, and M. Birch, "High-speed holographic optical tweezers using a ferroelectric liquid crystal microdisplay," *Optics Express*, vol. 11, pp. 1–7, 2003.

[147] Z. M. Huang, Y. Z. Zhang, M. Kotaki, and S. Ramakrishna, "A review on polymer nanofibers by electrospinning and their applications in nanocomposites," *Compos. Sci. Technol.*, vol. 63, pp. 2223–2253, 2003.

[148] B. Zhang, J. He, X. Li, F. Xu, and D. Li, "Micro/nanoscale electrohydrodynamic printing: from 2D to 3D," *Nanoscale*, vol. 8, pp. 15376–15388, 2016.

[149] J. A. Lewis, "Direct ink writing of 3D functional materials," *Adv. Funct. Mater.*, vol. 16, pp. 2193–2204, 2006.

[150] N.-S. Kim and K. N. Han, "Future direction of direct writing," *J. Appl. Phys.*, vol. 108, Art no. 102801, 2010.

[151] L. Wu, Z. Dong, F. Li, H. Zhou, and Y. Song, "Emerging progress of inkjet technology in printing optical materials," *Adv. Opt. Mater.*, vol. 4, pp. 1915–1932, 2016.

[152] D. Wang, X. Zhao, Y. Lin, et al., "Fabrication of micro/nano-structures by electrohydrodynamic jet technique," *Front. Mech. Eng.*, vol. 12, 477–489, 2017.

[153] Y. Han and J. Dong, "Electrohydrodynamic printing for advanced micro/nanomanufacturing: current progresses, opportunities, and challenges," *J. Micro Nano-Manufacturing*, vol. 6, 2018, https://doi.org/10.1115/1.4041934.

[154] B. Zhang, J. He, Q. Lei, and D. Li, "Electrohydrodynamic printing of sub-microscale fibrous architectures with improved cell adhesion capacity," *Virtual Phys. Prototyp.*, vol. 15, pp. 62–74, 2020.

[155] J. U. Park, M. Hardy, S. J. Kang, et al., "High-resolution electrohydrodynamic jet printing," *Nat. Mater.*, vol. 6, pp. 782–789, 2007.

[156] Y. Liang, J. Yong, Y. Yu, et al., "Direct electrohydrodynamic patterning of high-performance all metal oxide thin-film electronics," *ACS Nano*, vol. 13, pp. 13957–13964, 2019.

[157] F. D. Prasetyo, H. T. Yudistira, V. D. Nguyen, and D. Byun, "Ag dot morphologies printed using electrohydrodynamic (EHD) jet printing based on a drop-on-demand (DOD) operation," *J. Micromech. Microeng.*, vol. 23, Art no. 095028, 2013.

[158] J. O. Hardin, T. J. Ober, A. D. Valentine, and J. A. Lewis, "Microfluidic printheads for multimaterial 3D printing of viscoelastic inks," *Adv. Mater.*, vol. 27, pp. 3279–3284, 2015.

[159] R. E. Saunders, J. E. Gough, and B. Derby, "Delivery of human fibroblast cells by piezoelectric drop-on-demand inkjet printing," *Biomaterials*, vol. 29, pp. 193–203, 2008.

[160] G. M. Gratson, F. García-Santamaría, V. Lousse, et al., "Direct-write assembly of three-dimensional photonic crystals:

conversion of polymer scaffolds to silicon hollow-woodpile structures," *Adv. Mater.* 18, pp. 461–465, 2006.

[161] F. D. Ruz-Nuglo and L. J. Groven, "3-D printing and development of fluoropolymer based reactive inks," *Adv. Eng. Mater.* 20, Art no. 1700390, 2018.

[162] C. Ladd, J.-H. So, J. Muth, and M. D. Dickey, "3D Printing of free standing liquid metal microstructures," *Adv. Mater.* 25, pp. 5081–5085, 2013.

[163] M. A. Skylar-Scott, S. Gunasekaran, and J. A. Lewis, "Laserassisted direct ink writing of planar and 3D metal architectures," *Proc. Natl. Acad. Sci.*, vol. 113, pp. 6137–6142, 2016.

[164] L. Hirt, A. Reiser, R. Spolenak, and T. Zambelli, "Additive manufacturing of metal structures at the micrometer scale," *Adv. Mater.*, vol. 29, Art no. 1604211, 2017.

[165] R. Wang, W. Yang, P. Zhu, S. Gao, B. Li, and Q. Li, "Creation of 3D terahertz photonic crystals by the direct writing technique with a TiO_2 sol-gel ink," *J. Am. Ceram. Soc.*, vol. 101, pp. 1967–1973, 2018.

[166] P. Zhu, W. Yang, R. Wang, S. Gao, B. Li, and Q. Li, "Direct writing of flexible barium titanate/polydimethylsiloxane 3D photonic crystals with mechanically tunable terahertz properties," *Adv. Opt. Mater.*, vol. 5, Art no. 1600977, 2017.

[167] J. A. Lewis, J. E. Smay, J. Stuecker, and J. Cesarano, "Direct ink writing of three-dimensional ceramic structures," *J. Am. Ceram. Soc.*, vol. 89, pp. 3599–3609, 2006.

[168] S. H. Park, R. Su, J. Jeong, et al., "3D printed polymer photodetectors," *Adv. Mater.*, vol. 30, Art no. 1803980, 2018.

[169] S. T. Parker, P. Domachuk, J. Amsden, et al., "Biocompatible silk printed optical waveguides," *Adv. Mater.*, vol. 21, pp. 2411– 2415, 2009.

[170] D. B. Kolesky, R. L. Truby, A. S. Gladman, T. A. Busbee, K. A. Homan, and J. A. Lewis, "3D bioprinting of vascularized, heterogeneous cell-laden tissue constructs," *Adv. Mater.*, vol. 26, pp. 3124–3130, 2014.

[171] D. B. Kolesky, K. A. Homan, M. A. Skylar-Scott, and J. A. Lewis, "Three-dimensional bioprinting of thick vascularized tissues," *Proc. Natl. Acad. Sci.*, vol. 113, pp. 3179–3184, 2016.

[172] P. Galliker, J. Schneider, H. Eghlidi, S. Kress, V. Sandoghdar, and D. Poulikakos, "Direct printing of nanostructures by electrostatic autofocussing of ink nanodroplets," *Nat. Commun.*, vol. 3, pp. 1–9, 2012.

[173] J. Schneider, P. Rohner, D. Thureja, M. Schmid, P. Galliker, and D. Poulikakos, "Electrohydrodynamic nanodrip printing of high aspect ratio metal grid transparent electrodes," *Adv. Funct. Mater.*, vol. 26, pp. 833–840, 2016.

[174] B. W. An, K. Kim, H. Lee, et al., "High-resolution printing of 3D structures using an electrohydrodynamic inkjet with multiple functional inks," *Adv. Mater.*, vol. 27, pp. 4322–4328, 2015.

[175] D. Wang, X. Zhao, Y. Lin, et al., "Nanoscale coaxial focused electrohydrodynamic jet printing," *Nanoscale*, vol. 10, pp. 9867–9879, 2018.

[176] M. J. Grotevent, C. U. Hail, S. Yakunin, et al., "Nanoprinted quantum dot–graphene photodetectors," *Adv. Opt. Mater.*, vol. 7, Art no. 1900019, 2019.

[177] J. Park, J. Moon, H. Shin, D. Wang, and M. Park, "Directwrite fabrication of colloidal photonic crystal microarrays by ink-jet printing," *J. Colloid. Interface. Sci.*, vol. 298, pp. 713–719, 2006.

[178] W. Shen, M. Li, C. Ye, L. Jiang, and Y. Song, "Direct-writing colloidal photonic crystal microfluidic chips by inkjet printing for label-free protein detection," *Lab Chip*, vol. 12, pp. 3089–3095, 2012.

[179] J. Wang, L. Wang, Y. Song, and L. Jiang, "Patterned photonic crystals fabricated by inkjet printing," *J. Mater. Chem. C*, vol. 1, pp. 6048–6058, 2013.

[180] D. J. Lorang, D. Tanaka, C. M. Spadaccini, K. A. Rose, N. J. Cherepy, and J. A. Lewis, "Photocurable liquid core–fugitive shell printing of optical waveguides," *Adv. Mater.*, vol. 23, pp. 5055–5058, 2011.

[181] C. Zhang, C. L. Zou, Y. Zhao, et al., "Organic printed photonics: from microring lasers to integrated circuits," *Sci. Adv.*, vol. 1, 2015, https://doi.org/10.1126/sciadv.1500257.

[182] B. H. Kim, M. S. Onses, J. B. Lim, et al., "High-resolution patterns of quantum dots formed by electrohydrodynamic jet printing for light-emitting diodes," *Nano Lett.*, vol. 15, pp. 969–973, 2015.

[183] Y. L. Kong, I. A. Tamargo, H. Kim, et al., "3D printed quantum dot light- emitting diodes," *Nano Lett.*, vol. 14, pp. 7017–7023, 2014.

[184] P. Yang, L. Zhang, D. J. Kang, R. Strahl, and T. Kraus, "High-resolution inkjet printing of quantum dot light- emitting microdiode arrays," *Adv. Opt. Mater.*, vol. 8, Art no. 1901429, 2020.